Environmental influences on the morphology and dynamics of group-sized haloes

Cinthia Ragone-Figueroa[1,2]★ and Manolis Plionis[3,4]

[1]*Grupo de Investigaciones en Astronomía Teórica y Experimental, IATE, Observatorio Astronómico, Laprida 854, 5000 Córdoba, Argentina*
[2]*Consejo de Investigaciones Científicas y Técnicas de la República, Argentina*
[3]*Institute of Astronomy & Astrophysics, National Observatory of Athens, Palaia Penteli 152 36, Athens, Greece*
[4]*Instituto Nacional de Astrofísica Optica y Electrónica, AP 51 y 216, 72000 Puebla, México*

ABSTRACT

We use group-sized haloes, with masses in the range $10^{13} < M < 2 \times 10^{14} \, h^{-1} \, M_\odot$, identified with a 'friends of friends' (FOF) algorithm in a concordance Λ cold dark matter (ΛCDM) GADGET2 (dark matter only) simulation to investigate the dependence of halo properties on the environment at $z = 0$. The study is carried out using samples of haloes at different distances from their nearest massive *cluster* halo, considered as such if its mass is larger than the upper limit of the above halo mass range (i.e. $M \geqslant 2 \times 10^{14} \, h^{-1} \, M_\odot$). We find that the fraction of haloes with substructure typically increases in high-density regions. The halo mean axial ratio $\langle c/a \rangle$ also increases in overdense regions, a fact which is true for the whole range of halo mass studied. This can be explained as a reflection of an earlier halo formation time in high-density regions, which gives haloes more time to evolve and become more spherical. Moreover, this interpretation is supported by the fact that, at a given halo–cluster distance, haloes with substructure are more elongated than their equal mass counterparts with no substructure, reflecting that the virialization (and thus sphericalization) process is interrupted by merger events. The velocity dispersion of low-mass haloes with strong substructure shows a significant increase near massive clusters with respect to equal mass haloes with low levels of substructure or with haloes found in low-density environments. The alignment signal between the shape and the velocity ellipsoid principal axes decreases going from lower to higher density regions, while such an alignment is stronger for haloes without substructure. We also find, in agreement with other studies, a tendency of halo major axes to be aligned and of minor axes to lie roughly perpendicular with the orientation of the filament within which the halo is embedded, an effect which is stronger in the proximity of the massive clusters.

Key words: methods: *N*-body simulations – galaxies: clusters: general – galaxies: haloes – dark matter.

1 INTRODUCTION

According to the current cold dark matter (CDM) paradigm, haloes emerging from a Gaussian primordial density fluctuation field, assemble through gravitational processes to form larger systems which eventually virialize. These structures evolve in a hierarchical fashion aggregating smaller mass systems, flowing out of voids and along filaments, giving rise to deep potential wells, the cluster of galaxies. The role that the environment plays in modifying the properties of the smaller systems, such as galaxies, is being exhaustively studied and it is well known that many of the observed galaxy properties

correlate strongly with environment (e.g. Dressler 1980; Goto 2003; see Boselli & Gavazzi 2006, for a recent review). The properties of the galaxy group-sized haloes within which they are embedded could also vary as a function of environment, since mergers and tidal interactions are more probable in high-density environments.

The proximity of a galaxy or a group-sized halo to a massive attractor, like a cluster, and the corresponding strong gravitational interactions not only with the cluster itself but also with its local surrounding, which is denser near the cluster, might affect halo properties such as, among others, shape, size, concentration, orientation, velocity dispersion, amount of substructure and internal alignments (for examples of such observational evidence, see Schuecker et al. 2001; Plionis & Basilakos 2002; Plionis 2004; Martínez & Muriel 2006). Quantifying such effects in numerical simulations and

★E-mail: cin@mail.oac.uncor.edu

understanding their significance could help understand the physical processes that act to determine the properties of galaxies as a function of their environment.

However, one should also remember that differences between galaxy and group haloes, in high- and low-density regions, could also arise as a natural consequence of cosmological initial conditions, like halo formation time (e.g. Gottlöber, Klypin & Kratsov 2001; Sheth & Tormen 2004) or halo spin generation efficiency as a function of local density (Lee 2006).

Various recent studies have applied environment detecting algorithms in an attempt to characterize the diversity of cosmic environments from voids, to walls, filaments and clusters and thus facilitate the study of environmental effects on galaxy, group and cluster properties. Such algorithms are based on a variety of pattern recognition techniques from the simplest local overdensity measures to more elaborate techniques based on second-order local variations of the density field (e.g. Colberg, Krughoff & Connolly 2005; Pimbblet 2005; Stoica et al. 2005; Aragón-Calvo et al. 2007; Hahn et al. 2007).

Lemson & Kauffmann (1999) explored the effect of environment on different halo properties like their mass function, concentration parameter, formation redshift, spin parameter and shape and found that halo mass is the only property that correlates significantly with local environment. It is important to note that the variation of the halo mass function in different environments, i.e., the fact that high-mass haloes are underrepresented and overrepresented in low- and high-density regions, respectively, suggests that any apparent dependence of halo properties on the environment could be a consequence of the dependence of these properties on halo mass. Therefore, one needs to disentangle the two dependences and to perform any environmental dependence study as a function of halo mass as well.

A large number of recent studies on the environmental effects on a variety of halo properties, like halo shapes, spin, alignments velocity dispersion, and for different mass halo ranges, have been presented (e.g. Faltenbacher et al. 2002; Einasto et al. 2003, 2005; Ragone et al. 2004; Avila-Reese et al. 2005; Hopkins, Bahcall & Bode 2005; Altay, Colberg & Croft 2006; Basilakos et al. 2006; Plionis, Ragone-Figueroa & Basilakos 2006; Aragón-Calvo et al. 2007; Hahn et al. 2007; Maulbetsch et al. 2007). However, results of different studies are not always in agreement with each other, a fact that could be due to different quantifications of the environment or due to different analysis tools. For example, Einasto et al. (2005) found that group and cluster-sized DM haloes, in high-density regions, have smaller eccentricities (are more spherical) than in low-density regions, while Kasun & Evrard (2005) have found no such dependence. Similarly, Avila-Reese et al. (2005) and Hahn et al. (2007) have found a dependence of galaxy-sized DM haloes shapes on environment but again no such obvious dependence for larger DM haloes.

An interesting property to study as a function of environment is the internal alignment between the principal axes of the shape and velocity anisotropy ellipsoids, which can be considered as an indication of relaxation in a system where the shape is supported by internal velocities (e.g. Tormen 1997). Kasun & Evrard (2005) and Allgood et al. (2006) found for cluster-sized DM haloes a good such alignment, although no investigation in different environments has been reported. Furthermore, the external alignment between DM halo axes or angular momentum and the orientation of the filament in which the halo is embedded is of interest. Bailin & Steinmetz (2005) found a very strong tendency for the halo minor axis to lie perpendicular to the large-scale filament, but a much weaker tendency for the major axis to be oriented parallel to it. They also found that the

group- and cluster-sized halo angular momenta lie perpendicular to the large-scale filaments, while that of galaxy-sized haloes tend to lie parallel to them. This suggests that group-sized DM haloes acquire most of their angular momenta from mergers along the filament direction. Avila-Reese et al. (2005) in turn find a decreasing alignment signal between minor axis and angular momentum of galaxy-sized DM haloes going from overdense to underdense regions.

In this work we attempt to give a new insight in the behaviour of group-sized DM halo properties (shape, velocity dispersion, internal and external alignments) as a function of environment, taking special care to disentangle their correlation with halo mass, as mentioned before. We also divide our sample of group-sized haloes according to the amount of substructure that they have, in order to infer if mergers and/or gravitational tidal interactions play a significant role in shaping the DM halo morphological and dynamical properties.

The outline of this paper is as follows. In Section 2 we describe the numerical simulation method, the halo identification procedure and the research methodology that we will follow. In Section 3, we present the methods for the computation of the shape and velocity tensors, the angular momentum and alignment measures, and finally we present a thorough study for the quantification that we use to determine the halo substructure. In Section 4 we study the dependence of halo shape and dynamics on environment, while in Section 5 we present the corresponding study of internal and external halo alignments. Finally, we summarize our results and draw our conclusions in Section 6.

2 NUMERICAL DATA AND RESEARCH METHODOLOGY

The numerical simulations used in this work were performed using the GADGET2 code (Springel 2005) with dark matter only. This parallel code was run in a Beowulf cluster with 32 Intel Xeon processors (3.06 GHz). The cosmological parameters used correspond to a flat cosmological model with a non-vanishing cosmological constant (ΛCDM): $\Omega_{\rm m} = 0.3$, $\Omega_{\Lambda} = 0.7$, $\sigma_8 = 0.9$, $h = 0.72$, where $\Omega_{\rm m}$ and Ω_{Λ} are the present day matter and vacuum energy densities in units of the critical density, σ_8 is the present linear rms amplitude of mass fluctuation in spheres of $8\,h^{-1}$ Mpc and h is the Hubble parameter in units of $100\,{\rm km\,s^{-1}\,Mpc^{-1}}$. The initial conditions are generated with the GRAFIC2 package (Bertschinger 2001), which also computes the transfer function as described in Ma & Bertschinger (1995).

The main simulation was run in a cube of size $L = 500\,h^{-1}$ Mpc, using 512^3 particles. The particle mass is $\sim 7.7 \times 10^{10}\,h^{-1}\,{\rm M_\odot}$ and the force softening length is $\epsilon = 100\,h^{-1}$ kpc. Individual particle time-steps are chosen to be proportional to the square root of the softening length over the acceleration $\boldsymbol{a}$: $\Delta t_i = \sqrt{2\eta\epsilon/|\boldsymbol{a}|}$. We set the dimensionless parameter which controls the accuracy of the time-step to be $\eta = 0.02$.

The haloes were identified using a friends of friends (FOF) algorithm with a linking length $l = 0.17$ times the mean interparticle separation. Given the purposes of this work, we only use haloes with at least 130 particles, i.e., with masses greater than $10^{13}\,h^{-1}\,{\rm M_\odot}$. Note that this halo finder does not identify (for a given linking length) subhaloes belonging to larger *parent* haloes. For the purpose of our study, however, we will consider haloes with and without substructure (see further below), which in effect correspond to those haloes with or without relatively massive subhaloes.

The resulting sample of $\sim$58 000 haloes was split into two subsamples: haloes with masses $M > 2 \times 10^{14}\,h^{-1}\,{\rm M_\odot}$ are considered as *clusters* (in total 1598 haloes), whereas haloes in the range
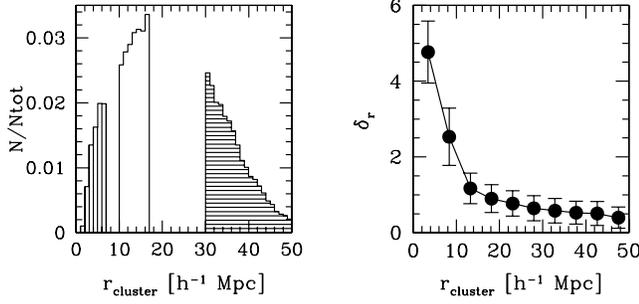
Figure 1. Left-hand panel: fraction of haloes in the H_{0-7} (vertical dashed histogram), H_{10-17} (empty histogram) and H_{30-50} (horizontal dashed histogram) sample. Right-hand panel: the median density contrast $\delta(r)$ computed in spheres of radius $8\,h^{-1}$ Mpc, as a function of r_{cluster} distance. Error bars represent the 33 and 67 per cent quantiles of the corresponding distribution.

$10^{13} < M < 2 \times 10^{14}\,h^{-1}\,\text{M}_\odot$ are considered as *groups* (56699 haloes).

In order to investigate the role that environment plays in determining halo properties, we find for each halo the distance to its nearest cluster and divide the halo sample in three subsamples according to this distance (r_{cluster}).

(i) Small distance subsample: $r_{\text{cluster}} < 7\,h^{-1}$ Mpc (H_{0-7}, hereafter ~8 per cent of the group sample).

(ii) Intermediate distance subsample: $10\,h^{-1}$ Mpc $< r_{\text{cluster}} < 17\,h^{-1}$ Mpc (H_{10-17} hereafter, ~21 per cent of the group sample).

(iii) Large distance subsample: $30\,h^{-1}$ Mpc $< r_{\text{cluster}} < 50\,h^{-1}$ Mpc (H_{30-50} hereafter, ~22 per cent of the group sample).

The left-hand panel of Fig. 1 shows the fraction of haloes in each one of the previously defined subsamples. In order to ensure that r_{cluster} is defining accurately the environment, we also compute for our haloes at different distances from the clusters the corresponding density contrast $\delta(r) = \rho(r)/\bar{\rho} - 1$, where $\rho(r)$ is the density in a sphere of radius $8\,h^{-1}$ Mpc around the halo centres and $\bar{\rho}$ is the mean matter background density. Results are shown in the right-hand panel of Fig. 1 from which it is obvious that indeed the halo distance to its nearest cluster is related to the overdensity in which the halo is embedded.

Given the significant effect that mergers and interactions can have on the shapes and alignments of haloes, and the fact that in overdense regions the halo mass function is skewed towards the high-mass end (Lemson & Kauffmann 1999), we will present our results as a function of their:

(i) halo mass,

(ii) environment, determined by r_{cluster}, and

(iii) halo dynamical state, determined by the Dressler & Shectman (1988) method (see the next section).

Therefore, any dependence of the halo properties on environment will be disentangled from the mass function effects, and will not be attributed to the overabundance of high-mass haloes in overdense regions.

For the purpose of testing the robustness of our substructure determination procedure to variations of the simulation resolution and box size, we also run (i) one simulation with the same resolution as the main simulation but in an eight times smaller box, i.e., evolving 256^3 particles in a $L = 250\,h^{-1}$ Mpc side box (LR hereafter), and (ii) a higher resolution simulation obtained by resimulating the $L = 125\,h^{-1}$ Mpc central box of the former with 256^3 particles and $\epsilon = 50\,h^{-1}$ kpc (HR hereafter), reaching a particle mass resolution of

$9.7 \times 10^9\,h^{-1}\,\text{M}_\odot$. We identify haloes in both the LR and HR simulations using a linking length $l = 0.17$ times the mean interparticle separation as in our main simulation.

3 DETERMINATION OF HALO SHAPE, ALIGNMENTS AND DYNAMICAL STATE

3.1 Parameter definition

The shape of haloes, modelled as ellipsoids, is determined by diagonalizing their inertia tensor

$$I_{ij} = \sum_N x_{i,n} x_{j,n}, \tag{1}$$

where N is the number of particles in the halo and $x_{i,n}$ is the ith component of the position vector of the nth particle relative to the halo centre. The principal axes of the fitted ellipsoid (a, b, c with $a \geqslant b \geqslant c$) are related to the square root of the eigenvalues of the inertia tensor. The corresponding eigenvectors provide the directions of the principal axes of the fitted ellipsoid.

Similarly, velocity moments are obtained by diagonalizing the velocity anisotropy tensor

$$V_{ij} = \sum_N v_{i,n} v_{j,n}, \tag{2}$$

where $v_{i,n}$ is the ith component of the velocity vector of the nth particle relative to the halo centre-of-mass velocity. Note that $a_{\text{vel}} \geqslant b_{\text{vel}} \geqslant c_{\text{vel}}$ will denote the major, middle and minor axes of the velocity ellipsoids, respectively.

We compute the specific angular momentum of each halo containing N particles as

$$\boldsymbol{L} = \frac{1}{N} \sum_N \boldsymbol{r}_i \times \boldsymbol{v}_i, \tag{3}$$

where $\boldsymbol{r}_i$ and $\boldsymbol{v}_i$ are the position and velocity vectors of the particle i relative to the halo centre of mass.

The various alignments between different pairs of vectors, representing either the principal axes of the halo density and velocity ellipsoid, the halo angular momentum or the direction to a neighbouring cluster halo, will be estimated by the mean of the distribution of $|\cos(\theta)|$, where θ is the angle between the directions of any two vectors, $\hat{\boldsymbol{v}}_1$ and $\hat{\boldsymbol{v}}_2$, we are interested in. Therefore,

$$\cos(\theta) = \hat{\boldsymbol{v}}_1 \cdot \hat{\boldsymbol{v}}_2. \tag{4}$$

Perfect alignment and anti-alignment correspond to $|\cos(\theta)| = 1$ and 0, respectively, whereas for the random three-dimensional case the expected distribution mean value is $\langle |\cos(\theta)| \rangle = 0.5$.

Finally, we use the Dressler & Shectman (1988) algorithm to estimate the amount of substructure in haloes. Briefly, this method determines the mean local velocity $\langle \boldsymbol{v}_{\text{loc}} \rangle$ and the local velocity dispersion σ_{loc} of the nearest n neighbours from each halo particle i and compares them with the mean velocity, $\langle \boldsymbol{V} \rangle$, and the velocity dispersion, σ, of the whole halo of N particles, defining the following measure:

$$\delta_i^2 = \frac{n}{\sigma} \left[(\langle \boldsymbol{v}_{\text{loc}} \rangle - \langle \boldsymbol{V} \rangle)^2 + (\sigma_{\text{loc}} - \sigma)^2 \right], \tag{5}$$

where

$$\sigma_{\text{loc}}^2 = \frac{\sum_n (\boldsymbol{v}_{\text{loc}} - \boldsymbol{v}_i)^2}{n - 1} \tag{6}$$

and

$$\sigma^2 = \frac{\sum_N (\langle \boldsymbol{V} \rangle - \boldsymbol{v}_i)^2}{N - 1}. \tag{7}$$

A quantification of the substructure present in a halo is given by the so-called Δ-*deviation*, which is the sum of the individual δ_i values over all halo particles N:

$$\Delta = \frac{\sum_N \delta_i}{N}. \tag{8}$$

The larger the Δ-deviation the stronger is the halo substructure. This statistic depends on the number of nearest neighbours n which is used in the analysis, and as we verified on the number of particles used to resolve a halo as well.

We have computed the Δ-deviation using two different values of n: (i) $n = 25$ as in Knebe & Müller (1999) and (ii) $n = N^{1/2}$ as in Pinkney et al. (1996) and find similar results.

3.2 Random and systematic parameter uncertainties

We investigate the uncertainty introduced by resolution effects in the determination of our morphological and dynamical halo parameters. The fact that low-mass haloes are resolved by a smaller number of particles with respect to higher mass haloes would inevitably create a random or possibly even a systematic deviation from their nominal values. To investigate these uncertainties, we use a procedure similar to that of Avila-Reese et al. (2005).

We perform 100 realizations of each massive halo (having more than 5000 particles) which we resolve selecting randomly the same number of particles as that of the lowest mass haloes used in our analysis (i.e. 130 random particles). For each realization we then compute the halo c/a axis ratio, velocity dispersion, velocity–shape major axes misalignment angle, $\hat{\boldsymbol{a}} \cdot \hat{\boldsymbol{a}}_{\text{vel}}$, and minor axis–angular momentum misalignment angle, $\hat{\boldsymbol{c}} \cdot \hat{\boldsymbol{L}}$.

The distributions of the 1σ deviations from their nominal value, plotted in Fig. 2, have mean values of ~ 9, 3.5, 16 and 30 per cent, respectively, for the c/a axis ratio (top left-hand panel), velocity

Figure 3. Left-hand panel: the dependence of the mean Δ-deviation substructure index on halo mass. The filled circles, connected with the solid line, represent the mean Δ-deviation computed using all the halo member particles, whereas the corresponding values choosing to have the same halo resolution, i.e. ~ 130 random particles per halo (Δ_{ran}), is shown as open circles connected with the dashed line. The estimated bootstrap uncertainties are smaller than the size of the symbols. Right-hand panel: the percentage of haloes with Δ-deviation higher than the mean value (i.e. haloes with substructure), as a function of halo mass. The solid line and filled symbols correspond to haloes selected using the global distribution of Δ-deviations, estimated using all halo particles, irrespective of the halo mass (variable halo particle resolution). The dashed line and open symbols correspond to haloes selected using the global distribution of Δ_{ran}-deviations, estimated using ~ 130 particles per halo, irrespective of the halo mass (same halo particle resolution). While the dotted line shows the percentages of haloes with $\Delta > \langle \Delta_i \rangle$, evaluated within the ith bin of halo mass and using all halo particles.

dispersion (top right-hand panel), velocity–shape major axes misalignment angle (bottom left-hand panel) and minor axis–angular momentum misalignment angle (bottom right-hand panel). It is evident that the uncertainties are quite small, especially of the halo velocity dispersion, except for the misalignment angle, $\hat{\boldsymbol{c}} \cdot \hat{\boldsymbol{L}}$.

It is also possible that resolution effects do not only introduce a random error on the nominally defined shape and dynamical halo parameter. For example, for the case of the substructure index, Δ, a pronounced trend is apparent with $\langle \Delta \rangle$ increasing with halo mass. In Fig. 3 (left-hand panel), we show results based on the $n = N^{1/2}$ case (filled circles and solid line). There is an apparent monotonic increase of $\langle \Delta \rangle$ with halo mass. Furthermore, in the right-hand panel of Fig. 3 we show with the solid line, the percentage of haloes with Δ-deviation higher than the mean of the Δ distribution of all haloes ($\langle \Delta \rangle = 0.98$). Again, we see a monotonic increase of the fraction of haloes having substructure as a function of mass, with the most massive haloes appearing all to be substructured. These results create a suspicion that they could be due to the lower resolution with which the low-mass haloes are resolved. To investigate the resolution issue, we perform two tests:

(i) we compare the Δ-deviation index for the matching haloes of our HR and LR simulations, and

(ii) we recompute Δ for all mass haloes, but using only 130 randomly selected particles per halo (i.e. the same number resolution as in the smaller haloes).

Regarding the first test we select those pairs of haloes which match, in position and mass, in both the LR and HR halo samples. The masses of these matching haloes are allowed to differ only by 5 per cent, so as to ensure that we will compare properties of the same haloes with only difference their resolution (~ 8 times more particles in the HR matching haloes). We divide the matching haloes sample in three subsamples according to their masses, which are
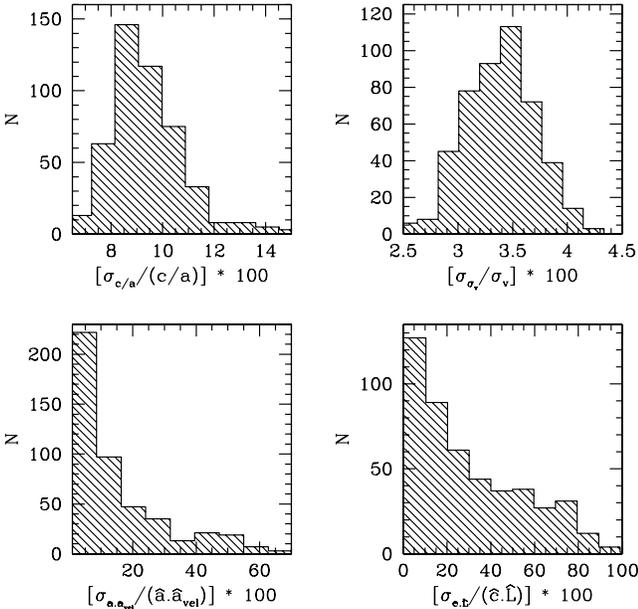
Figure 2. 1σ error distribution of the various dynamical and morphological parameters of haloes with more than 5000 particles but sampled with only 130 random particles (100 realizations are used). The distributions of the halo axial ratios, velocity dispersions, velocity–shape major axes misalignment angles and minor axis–angular momentum misalignment angles are shown in the top left, top right, bottom left and bottom right-hand panels, respectively.
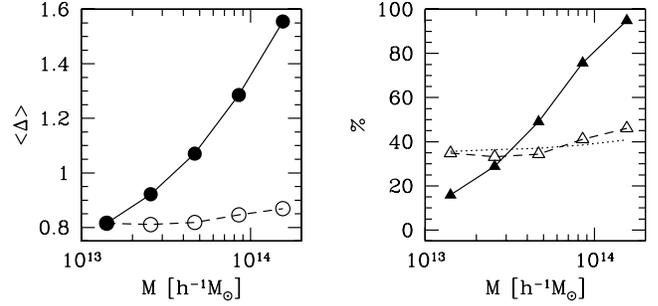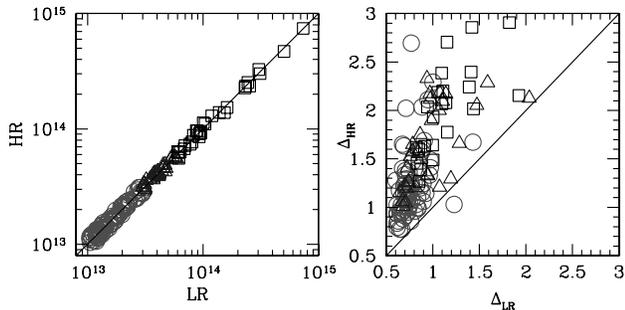
Figure 4. Left-hand panel: comparison of the masses of matching LR and HR haloes: open circles, triangles and squares correspond to haloes with masses $10^{13} < M < 3 \times 10^{13} \, h^{-1} \, \mathrm{M}_\odot$, $3 \times 10^{13} < M < 6 \times 10^{13} \, h^{-1} \, \mathrm{M}_\odot$ and $6 \times 10^{13} < M < 10^{15} \, h^{-1} \, \mathrm{M}_\odot$, respectively. Right-hand panel: the Δ-deviation comparison of the matched LR and HR haloes.

compared in the left-hand panel of Fig. 4. In the right-hand panel, we compare their corresponding Δ-deviation values, and in all cases we find that Δ is significantly larger when computed in the higher resolution haloes, a fact which is further enhanced for the more massive haloes. This result verifies our suspicion that resolution effects could be the cause of the monotonic increase of Δ with halo mass.

We now continue with our second test and derive for each halo a new Δ-deviation index (Δ_{ran}) computed by using the same number of particles (130), randomly selected, in each halo independent of its mass. In this way we impose the same particle resolution on all haloes. Note that we use as Δ_{ran} the average over many realizations of the random particle selection process. The results of this procedure show that Δ_{ran} is systematically smaller than when using all the particles in the haloes, and increases very weakly with halo mass, as shown by the dashed line in both the left- and right-hand panels of Fig. 3. Again these results indicate the importance of resolution effects in quantifying the amount of halo substructure.

From our previous study, we have realized that the whole distribution of Δ-deviations shifts to higher values as a function of resolution. This translates to a shift at higher values of the Δ-deviation distribution as a function of halo mass, within the same simulation.

In the right-hand panel of Fig. 3 we also show, as the dotted line, the percentage of haloes as a function of halo mass, having their Δ estimated using all halo particles, but then selecting those with Δ larger than the mean, $\langle \Delta_{\mathrm{bin}} \rangle$, of the distribution within each bin of halo mass. It is evident from this plot that this case and the case based on Δ_{ran} give equivalent results. Had we not taken into account the resolution effects, we would have erroneously concluded that almost all massive haloes have strong substructure and that the opposite was true at the low halo mass end.

Given the computation of the substructure Δ-deviation index is more robust if all halo member particles are considered, we will refer from now on to haloes having substructure as those with $\Delta > \langle \Delta_{\mathrm{bin}} \rangle$ in the specific mass range bin which they belong.

The fraction of haloes with substructure, as defined before, are $\sim$45 per cent $\pm$ 5 per cent for the H_{0-7} haloes and 35 per cent $\pm$ 3 per cent for the H_{10-17} and H_{30-50} haloes, with only a weak dependence on halo mass. If, however, we select haloes nearer to massive clusters (i.e. $0 < r_{\mathrm{cluster}} < 4 \, h^{-1}$ Mpc), the fraction of low-mass haloes ($M < 2 \times 10^{13} \, h^{-1} \, \mathrm{M}_\odot$) with substructure grows to 65 per cent $\pm$ 3 per cent.

Note that haloes that went through a recent merger will have a higher Δ-deviation value with respect to those that either are isolated or had no recent merger event, thus having more time to virialize.

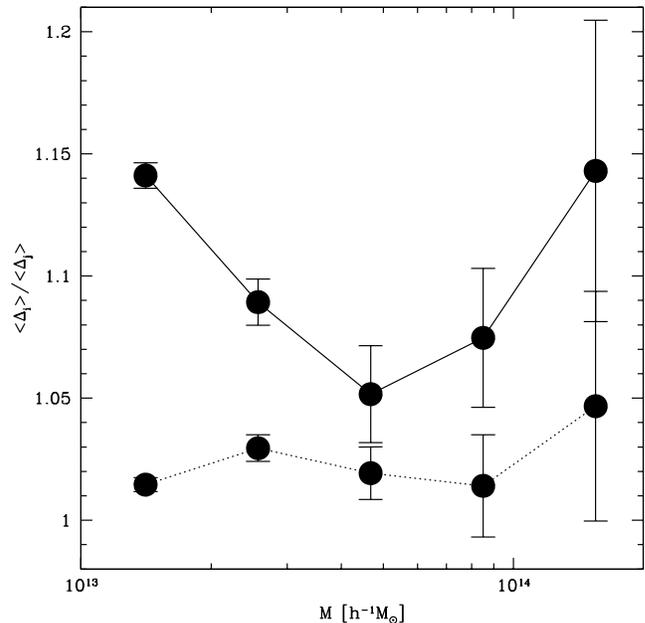**Figure 5.** Δ-deviation ratios as a function of halo mass and environment. The solid line represents the ratio: $\langle \Delta_{H_{0-7}} \rangle / \langle \Delta_{H_{30-50}} \rangle$, and the dotted line represents the ratio: $\langle \Delta_{H_{10-17}} \rangle / \langle \Delta_{H_{30-50}} \rangle$. Error bars are based on the propagation of the individual Δ-deviation uncertainties.

In Fig. 5 we present the dependence of the substructure index on the environment and halo mass. Solid and dotted lines stand for the ratios of Δ in the H_{0-7} and H_{10-17} samples, normalized to the most distant sample (H_{30-50}). As expected, we find haloes in the vicinity of massive clusters (solid line) to have larger Δ values (for their mass range) with respect to distant haloes (dotted line), presumably due to the higher merging rate and due to the stronger tidal field, found around overdense regions.

4 ENVIRONMENTAL EFFECTS ON HALO SHAPES AND DYNAMICS

4.1 Halo shape–mass correlation

In the ΛCDM cosmology, the dependence of shapes on DM halo mass has been well established in many recent studies with more massive haloes being less spherical, i.e., having a lower axis ratio, c/a (e.g. Bullock 2002; Jing & Suto 2002; Kasun & Evrard 2005; Allgood et al. 2006; Gottlöber & Turchaninov 2006; Paz et al. 2006; Bett et al. 2007; Macciò et al. 2007). This can be explained considering that in the hierarchical clustering of CDM haloes, smaller mass haloes form earlier on average than massive ones, and thus they have more time to evolve, virialize and become more spherical. We should also note that including baryonic physics has a significant effect on the shapes of haloes (e.g. Kazantzidis et al. 2004). In this section, we investigate whether this trend changes when considering groups in different environments. Such a difference has been noted by Avila-Reese et al. (2005) between galaxy-sized haloes found in clusters and in voids, and by Hahn et al. (2007) between haloes found in clusters and in filaments but only for small halo masses ($M \leqslant 2 \times 10^{12} \, \mathrm{M}_\odot$). We do not probe this mass range and therefore our analysis concentrates only on larger mass haloes, typical of groups and poor clusters of galaxies.
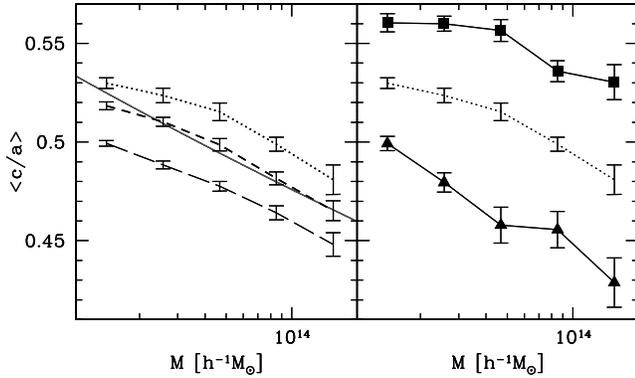
Figure 6. Left-hand panel: mean axial ratios $\langle c/a \rangle$ as a function of halo mass and environment. Dotted, short dashed and long dashed lines correspond to halo samples of different cluster–group distances (H_{0-7}, H_{10-17} and H_{30-50}, respectively). The standard deviation of the axial ratio distribution for the different halo subsamples and halo masses is between 0.11 and 0.12. Error bars were calculated using the bootstrap resampling technique. The solid line denotes the Allgood et al. (2006) fit. Right-hand panel: mean axial ratio $\langle c/a \rangle$, as a function of halo mass, only for the H_{0-7} haloes (dotted line). Squares and triangles correspond to H_{0-7} haloes with Δ-deviation values lower and higher than $\langle \Delta_{\rm bin} \rangle$, respectively.

Fig. 6 (left-hand panel) presents our results for the three $r_{\rm cluster}$ subsamples (H_{0-7}, H_{10-17} and H_{30-50}), with error bars computed using the bootstrap resampling technique. In all cases the trend we find is in accordance with the well-known mass–shape relation, with $\langle c/a \rangle$ increasing with decreasing halo mass. However, it is shifted towards more spherical axial ratios when considering haloes nearer to massive clusters. This can be explained by the fact that haloes in high-density environments are formed earlier than haloes, of the same mass range, in low-density environments (e.g. Sheth & Tormen 2004), giving the former more time to evolve, relax and hence become more spherical (Avila-Reese et al. 2005). This is in agreement with haloes at higher redshifts being more elongated than present day equal mass haloes (e.g. Allgood et al. 2006).

Another representation of our results is shown in Fig. 7, where we plot the c/a frequency distribution of well-resolved haloes (i.e. those with $3.8 \times 10^{13} < M < 10^{14}\,h^{-1}\,{\rm M}_{\odot}$). The means of these distributions are 0.50, 0.48 and 0.47 for the H_{0-7} (dashed histogram), H_{10-17} (dotted histogram) and H_{30-50} (empty histogram) samples, respectively, while a Kolmogorov–Smirnov two-sample test shows them to be different at a very high significant level.

We now consider only the H_{0-7} haloes and compute the shape–mass relation but separating haloes with high and low Δ-deviation (substructure). Results are plotted in the right-hand panel of Fig. 6, where squares correspond to haloes with $\Delta < \langle \Delta_{\rm bin} \rangle$ and triangles to haloes with $\Delta > \langle \Delta_{\rm bin} \rangle$. The shape–mass relation is basically maintained in both subsamples although: (i) it is much shallower for haloes in the low Δ-deviation subsample, and (ii) it is shifted towards lower $\langle c/a \rangle$ for haloes in the high Δ-deviation subsample. This result is indeed expected if to consider that more virialized systems tend to be more spherical. Those system with high level of substructure, which are dynamically younger systems, have interrupted their virialization process due to some recent merger event and therefore have a more elongated shape than systems with no sign of substructure. This latter behaviour is present in the whole range of considered masses and also in the H_{10-17} and H_{30-50} subsamples.

In order to discard the possibility that discreteness effects could impose the $\langle c/a \rangle$–mass correlation, we recomputed the halo shapes
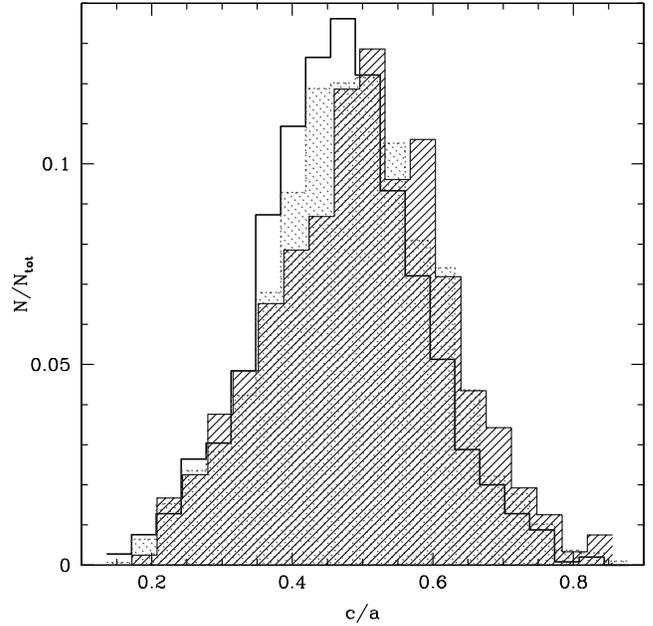

Figure 7. Axial ratio (c/a) distributions for haloes in the mass range 3.8×10^{13}–$10^{14}\,h^{-1}\,{\rm M}_{\odot}$. Shaded, dotted and empty histograms correspond to the H_{0-7}, H_{10-17} and H_{30-50} halo samples, whose means are 0.50, 0.48 and 0.47, respectively. The 1σ dispersion is in all cases ~ 0.1

but using realizations of only 130 randomly selected particles per halo, so as to resemble the resolution of the less massive haloes (see also Paz et al. 2006, for discreteness related effects). We indeed recover the same $\langle c/a \rangle$–mass trend and thus we verify that it is not imposed by the variable resolution with which the different mass haloes are resolved. However, there is a shift towards less spherical values when using the common halo resolution of 130 randomly selected particles per halo. The apparent curvature towards lower c/a values and at the low-mass end of the $\langle c/a \rangle$–mass relation apparently disappears when using the common halo resolution, and thus it should probably be attributed to the variable halo resolution.

4.2 Halo velocity dispersion–mass correlation

In Fig. 8 we present the halo velocity dispersion–mass correlation. Velocity dispersions were computed using formula 7. Such a correlation is expected from the virial theorem. In order to investigate the possible influence of the environment on this relation and hence on the reliability of using the virial theorem to estimate halo masses, we present in the left-hand panel of Fig. 8 results for the three halo $r_{\rm cluster}$ (H_{0-7}, H_{10-17} and H_{30-50}) subsamples and for an extra subsample with $r_{\rm cluster} < 4\,h^{-1}$ Mpc (dot–dashed line).

As expected from the virial relation, we find that larger mass haloes have higher velocity dispersions, for all the considered subsamples. However, there is a shift towards higher velocity dispersions of low-mass haloes found near clusters with respect to those found further away. This trend is stronger the nearer the low-mass halo is found to the cluster. However, for halo–cluster distances $\gtrsim 10\,h^{-1}$ Mpc there is no effect whatsoever.

To investigate whether the halo dynamical state relates to the halo velocity dispersion–mass correlation, we divide the H_{0-7} subsample, as in the previous section, to those with and without substructure. Results are shown in the right-hand panel of Fig. 8, where the dotted line stands for all the H_{0-7} haloes, squares and triangles for
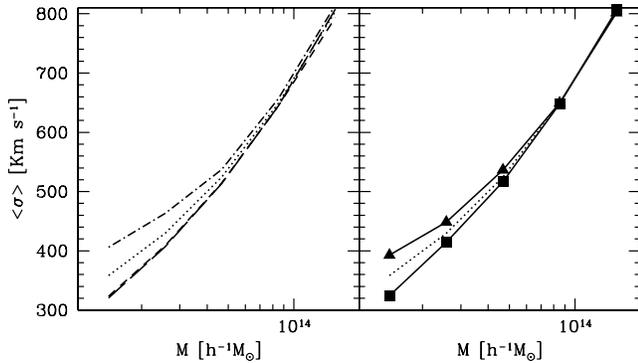
Figure 8. Mean velocity dispersion $\langle\sigma\rangle$ as a function of halo mass. Left-hand panel: results for the usual three $r_{cluster}$ subsamples (H_{0-7}, H_{10-17}, H_{30-50}), with line types already defined in Fig. 6, while the dot–dashed line corresponds to haloes with $r_{cluster} < 4\,h^{-1}$ Mpc (the H_{10-17} and H_{30-50} results are identical). Bootstrap errors are small, typically $\sim$10–20km s^{-1}. Right-hand panel: results only for the H_{0-7} halo subsample; Squares correspond to haloes with $\Delta < \langle\Delta_{bin}\rangle$ and triangles to haloes with $\Delta > \langle\Delta_{bin}\rangle$.

haloes with $\Delta < \langle\Delta_{bin}\rangle$ and $\Delta > \langle\Delta_{bin}\rangle$, respectively. There is indeed a dependence of the mass–velocity dispersion correlation on the amount of halo substructure but only for haloes with masses $\lesssim 5 \times 10^{13}\,h^{-1}\,M_{\odot}$, which are found to have a larger mean velocity dispersion than haloes with no or low levels of substructure. Note that Evrard et al. (2007) find similar results for what they call satellite haloes. Moreover, we find that haloes with a low Δ-deviation index behave similarly as haloes in the H_{10-17} and H_{30-50} samples (seen in the left-hand panel of Fig. 8), which show no dependence of the mean velocity dispersion on the presence or not of halo substructure. Note, however, that a slight shift towards higher velocity dispersion values is present also in high-mass haloes but only if choosing those haloes with extremely high Δ-deviation index.

4.3 Partial conclusions

These results, concerning the dependence of halo shapes and velocity dispersion on the halo dynamical state, give new insights in our understanding of halo formation and evolution.

Although the general expectation is that low-mass haloes in high-density environments formed earlier and thus should be relatively more virialized with respect to similar mass haloes in low-density regions, we have found a relatively high fraction of dynamically young and active haloes near massive clusters ($\gtrsim 45$ per cent). These haloes have in general a higher velocity dispersion (more evident at the low-mass end) and a lower $\langle c/a \rangle$ ratio with respect to similar mass virialized haloes. The high level of substructure of these haloes is probably because they are continuing to grow via mergers in the anisotropic outskirts of massive haloes (e.g. West 1994; Maulbetsch et al. 2007), although their dynamical state could also be affected from the strong tidal field imposed by their local high-density surrounding, while both cases imply a lower halo sphericity, as observed. The mergers as the most possible cause for the increase of the halo velocity dispersion is in agreement with Faltenbacher, Gottlöber & Mathews (2006) who find for an equal mass merging event (progenitors with masses $\sim 1 \times 10^{14}\,h^{-1}\,M_{\odot}$) an oscillatory behaviour of the velocity dispersion (among other properties). After the relaxation of the new system, the velocity dispersion is slightly larger, but it changes substantially during the event.

Now, higher mass haloes with a high Δ-deviation (substructure) in the vicinity of massive clusters also appear to be of lower spheric-

ity although, and contrary to the low-mass halo case, their velocity dispersion does not show any significant deviation from that of the more virialized high-mass haloes. This could be explained if typically the merger events, which alter the higher mass halo shape, are due to relatively lower mass haloes which although affect the overall shape, they affect less the dynamical structure of the high-mass halo, which is dominated by the main gravitational potential of the high-mass halo itself. It could also imply a faster 're-accommodation' of the velocity field with respect to the density field in the relatively deep principal halo potential well.

5 ENVIRONMENTAL EFFECTS ON HALO ALIGNMENTS

5.1 Internal halo alignments

In Section 1, we mentioned that there is a significant signal of alignment between the principal axes of the shape and the velocity anisotropy tensors, indicating that most of the haloes have their shapes supported by the velocities of their member particles (e.g. Tormen 1997; Kasun & Evrard 2005).

Here we investigate whether there is any environmental dependence on such an alignment effect. To this end we compute the mean absolute cosine of the angle between the major axes of the mentioned tensors, $\langle|\hat{a} \cdot \hat{a}_{vel}|\rangle$, as a function of the halo mass for the three halo subsamples (H_{0-7}, H_{10-17} and H_{30-50}).

In the left-hand panel of Fig. 9, we show the $\langle|\hat{a} \cdot \hat{a}_{vel}|\rangle$–mass correlation for the H_{0-7} (dotted line), H_{10-17} (dashed line) and H_{30-50} (long dashed line) samples. In all cases there is a good signal of alignment between the shape and velocity ellipsoid principal axes, especially for haloes at large distances from massive clusters (H_{10-17} and H_{30-50} subsamples), while within each subsample the alignment is stronger for the higher mass haloes. We have verified that this is not due to the variable resolution with which the different mass haloes are sampled.

Haloes at large distances from massive clusters have their velocity and shape better correlated probably because they are less tidally disrupted than in the high-density environment of the cluster, either by the cluster itself or/and by the local overabundance of lower mass haloes found in such environment. Even more so in the high-mass halo end probably because interactions and merging with
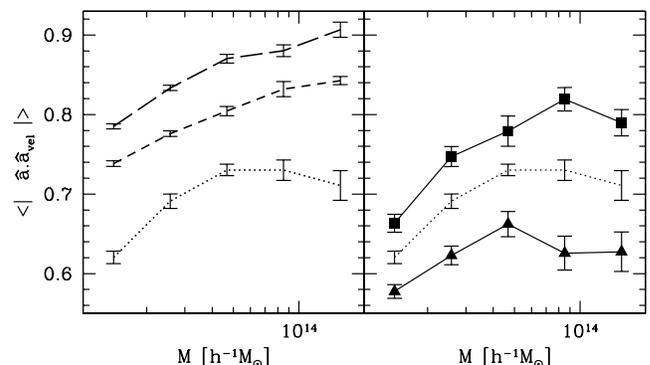

Figure 9. Left-hand panel: the direction cosine of the major axes of the shape and velocity ellipsoids $\langle|\hat{a} \cdot \hat{a}_{vel}|\rangle$ as a function of halo mass for the H_{0-7}, H_{10-17} and H_{30-50} halo subsamples. Line styles are as in Fig. 6. Error bars were calculated using the bootstrap resampling technique. Right-hand panel: the corresponding $\langle|\hat{a} \cdot \hat{a}_{vel}|\rangle$–mass correlation only for the H_{0-7} sample, split in those haloes with high level of substructure, $\Delta > \langle\Delta_{bin}\rangle$ (triangles), and those without substructure, $\Delta < \langle\Delta_{bin}\rangle$ (squares).

lower mass haloes can disturb minimally the phase space of these higher mass haloes. However, near the massive cluster (H_{0-7} subsample), the stronger halo–cluster gravitational interactions affect significantly the halo phase space and for this reason we observe a general decrease of the value of $\langle|\hat{a} \cdot \hat{a}_{\text{vel}}|\rangle$ for all halo masses.

This interpretation could be supported if those haloes with a high level of substructure showed even less aligned orientations. Indeed this is the case, as can be seen in the right-hand panel of Fig. 9, where we present for the H_{0-7} subsample the $\langle|\hat{a} \cdot \hat{a}_{\text{vel}}|\rangle$–mass correlation but split between haloes with high level of substructure, $\Delta > \langle\Delta_{\text{bin}}\rangle$ (triangles), and haloes with no substructure, $\Delta < \langle\Delta_{\text{bin}}\rangle$ (squares). The former haloes show a weaker alignment, as anticipated, suggesting that strong interactions and mergers introduce scatter in the phase space of these systems.

The segregation between haloes with and without substructure, seen in the right-hand panel of Fig. 9, is also present in the more distant halo samples (H_{10-17} and H_{30-50}). The same interpretation, given before, of the difference between equal mass haloes with and without substructure holds for these samples as well. Furthermore, the slightly better alignment seen for the more massive haloes is due to their deeper potential wells, which inevitably creates a better alignment.

Another internal alignment effect that we address is that between the directions of the angular momentum vector and the minor axis of the mass distribution, $|\hat{c} \cdot \hat{L}|$. It has been found that the angular momentum is most often aligned with the minor axis and perpendicular to the major axis (e.g. Dubinski 1992; Bailin & Steinmetz 2005; Bett et al. 2007). An environmental dependence has also been found by Avila-Reese et al. (2005) for galaxy-sized haloes, with a higher alignment signal in underdense regions (see also Hahn et al. 2007 for angular momentum orientations with large-scale structures).

Our results are shown in Fig. 10, where we also find such an alignment signal, although it is obvious that due to noise we are unable to detect different trends in the three halo subsamples. Note also that the amplitude of our alignment signal is significantly less than that found by Bailin & Steinmetz (2005), most probably because these authors define shapes using the reduced moment of inertia tensor, which weights strongly the inner parts of haloes, as well as because they choose to analyse only haloes of which both their small axis and angular momentum orientation have small uncertainties. Furthermore, one should keep in mind that, due to resolution effects (see
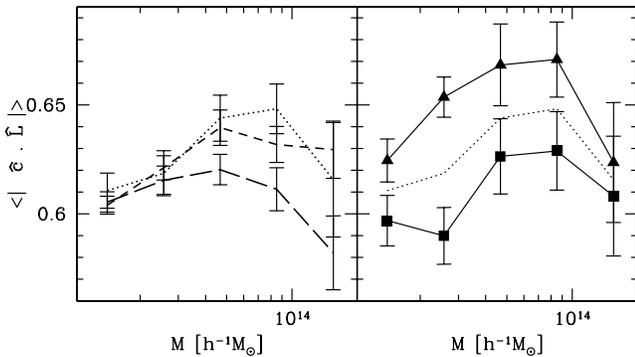
Section 3.2), the intrinsic uncertainty of this alignment measure is quite large for low-mass haloes.

Returning to our results we do find a systematic, although weak, trend of a better alignment for the H_{0-7} subsample (left-hand panel of Fig. 10), which is in the opposite direction than the results of Avila-Reese et al. (2005) based on galaxy-sized haloes. However, our haloes are much larger (groups and poor cluster size) and this could well be the reason of the apparent discrepancy. Furthermore, we are in general agreement with the recent results of Aragón-Calvo et al. (2007).

Moreover, haloes with high level of substructure seem to have $\hat{L}$ and $\hat{c}$ better correlated (right-hand panel Fig. 10), a fact which is true for all halo subsamples (H_{0-7}, H_{10-17} and H_{30-50}). This should be partly attributed to the fact that haloes with substructure are more elongated than relaxed haloes and thus they have both their angular momentum and minor axis vectors better defined. Furthermore, this result also implies that mergers probably affect significantly the angular momentum of haloes (e.g. Vitvitska et al. 2002), which gain part of their angular momentum from mergers preferentially occurring along the plane defined by the major and median axes.

5.2 External alignments

It has been shown that the orientation of the halo major axis is strongly correlated with the direction from which the last major merger event occurred (van Haarlem & van de Weygaert 1993). Therefore, it should be expected to find a correlation between halo major axis orientation and the direction defined by the halo–cluster distance, which in turn should indicate the orientation of the filament. Such alignment effects, among relatively massive haloes, have been found to be particularly strong and extending up to $\gtrsim 100\,h^{-1}$ Mpc (e.g. Faltenbacher et al. 2002; Hopkins et al. 2005; Kasun & Evrard 2005).

Here we also wish to calculate the alignment between the direction of each halo to their nearest cluster ($\hat{d}_{\text{gh}}$) and the halo major or minor axis orientation ($\langle|\hat{d}_{\text{gh}} \cdot \hat{a}|\rangle$ and $\langle|\hat{d}_{\text{gh}} \cdot \hat{c}|\rangle$, respectively) for all three (H_{0-7}, H_{10-17} and H_{30-50}) halo subsamples. The left-hand panel of Fig. 11 shows the case for the major axis alignment, while the left-hand panel of Fig. 12 shows the corresponding minor axis alignment case. As expected, the former alignment effect is strong, more so for haloes found near their clusters and for the high-mass haloes.
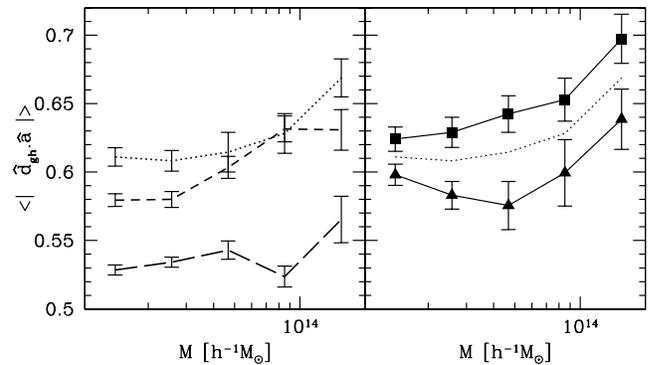
Figure 10. Left-hand panel: the direction cosine between the angular momentum and the minor axis $\langle|\hat{c} \cdot \hat{L}|\rangle$ as a function of halo mass for the H_{0-7}, H_{10-17} and H_{30-50} halo subsamples. Right-hand panel: the corresponding $\langle|\hat{c} \cdot \hat{L}|\rangle$–mass correlation only for the H_{0-7} sample, split in those haloes with high level of substructure, $\Delta > \langle\Delta_{\text{bin}}\rangle$ (triangles), and those without substructure, $\Delta < \langle\Delta_{\text{bin}}\rangle$ (squares).

Figure 11. Left-hand panel: correlation between halo–cluster direction and halo major axis orientation ($\langle|\hat{d}_{\text{gh}} \cdot \hat{a}|\rangle$) as a function of halo mass. Long dashed, short dashed and dotted lines correspond to different bins of cluster–group distances as in Fig. 6. Error bars were calculated using the bootstrap resampling technique. Right-hand panel: similar but only for the H_{0-7} sample, split into haloes with and without significant substructure, $\Delta > \langle\Delta_{\text{bin}}\rangle$ (triangles) and $\Delta < \langle\Delta_{\text{bin}}\rangle$ (squares), respectively.
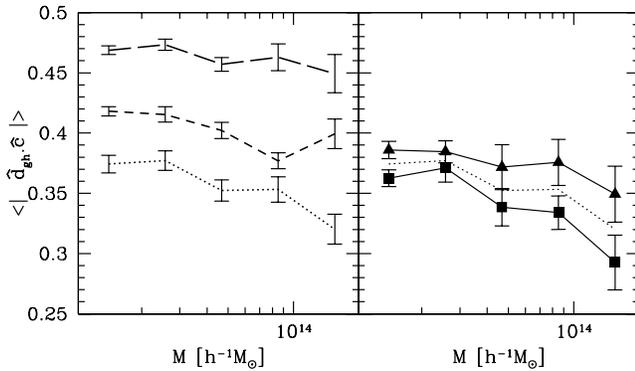
Figure 12. Left-hand panel: correlation between cluster–group direction and halo minor axis orientation ($\langle|\hat{d}_{gh} \cdot \hat{c}|\rangle$) as a function of halo mass. Right-hand panel: similar but only for the H_{0-7} sample, split into haloes with and without significant substructure.

As in Bailin & Steinmetz (2005), we find that the halo minor axes are in general anti-aligned (perpendicular) to the filament direction, again more so for haloes found near their clusters and for high-mass haloes. Now dividing our H_{0-7} subsample into those haloes with and without substructure (right-hand panels of Figs 11 and 12), we find very interesting results.

(i) Relatively virialized haloes, having no significant substructure, show a strong tendency for major axis alignment (and minor axis anti-alignment) with the direction to their nearest massive cluster implying that they retain strong memory of the initial anisotropic distribution from which they accreted matter (e.g. van Haarlem & van de Weygaert 1993).

(ii) Haloes with high level of substructure show a similar, although relatively weaker, alignment effect, which appears to be in disagreement with what one would naively expect given that mergers happen preferentially along the filaments. However, once a merger has happened, non-linear gravitational effects take place and until the merged structure relaxes, it may well appear less aligned with the filament orientation. Specially, low-mass haloes, being also small in size, interacting with other neighbouring haloes in the high-density surroundings of a massive cluster, could be relatively more affected by local gravitational effects which may not necessarily reflect the large-scale anisotropic distribution of matter in the filament.

An interesting complication in the above interpretation is that the halo angular momentum and minor axis is better aligned in high Δ-deviation haloes (see Section 5.1) and if directional mergers are responsible for such an alignment, being more frequent in the filament direction, then one might have expected their major axes to be more aligned with the halo–cluster direction than for virialized haloes (small Δ-deviations). However, what the angular momentum–minor axis halo alignment actually implies, in the above picture, is that the direction of the merger is in the plane defined by the major and medium axes and not necessarily along the major axis, which is not in contradiction with the above.

6 DISCUSSION AND CONCLUSIONS

We have used haloes identified with a FOF algorithm in a dark matter only ΛCDM simulation to study the dependence of the shape, dynamical state and various alignments of group-sized haloes on the halo environment. The smallest haloes analysed have at least 130 particles ($M \gtrsim 10^{13}\,h^{-1}\,\mathrm{M}_\odot$). In order to investigate if there is some

influence of the environment on the properties of haloes, we split the group sample into three subsamples according to their distances to the nearest massive *cluster* halo. We have also investigated the Dressler & Shectman (1988) algorithm, used to determine whether a halo has a high level of substructure or not, considered as an indication of their dynamical state, and we devised a substructure characterization of the haloes which is free of halo resolution effects. We then divide the haloes to those with and without a high level of substructure.

Our results can be summarized in the following.

(i) The well-known relation between halo shape and halo mass has also an environmental dependence, albeit weak. Haloes found at small distances from their massive cluster show a systematic shift towards larger axial ratios (i.e. they are more spherical) with respect to equal mass haloes at larger distances, a fact which is true for the whole range of halo masses studied. This result appears to be in disagreement with Hahn et al. (2007).

(ii) The velocity dispersion of equal mass haloes shows a dependence on the environment. Haloes with substructure, near massive clusters, have a larger velocity dispersion with respect to equal mass haloes with no or low-substructure index. This is probably due to the higher halo merging rate in high-density environments. On the contrary, haloes found further away do not exhibit this same behaviour: the velocity dispersion–mass trend is the same independent of the presence or not of substructure. The velocity dispersion of high-mass haloes does not seem to be affected by the environment, nor that of any halo at a distance larger than $\sim 10\,h^{-1}$ Mpc from its nearest massive cluster.

(iii) The influence of environment is also reflected in the internal alignment of the velocity and density ellipsoid principal axes. Such an alignment is stronger for higher mass groups, probably due to the better definition of their shape given that these groups are more elongated than lower mass ones, while it is weaker near massive clusters, where the influence of the cluster and the high-density halo neighbourhood is stronger. It is even weaker for haloes with a high level of substructure, which reflects the fact that during a merger the halo phase space is significantly perturbed.

(iv) Angular momentum and minor axes of haloes are roughly aligned, even more so for haloes with substructure. This relation does not seem to depend strongly on environment. However, one should keep in mind that the uncertainty of this measure is quite large due to resolution effects.

(v) On larger scales, we detect alignments between the orientation of a halo and the direction to its nearest massive cluster, which probably reflects the orientation of the filament within which they are embedded. The halo minor/major axes appear perpendicular/parallel to the filament, while the signal for both alignments is stronger for haloes near massive clusters and for haloes with no substructure.

(vi) Overall we have found that the halo properties studied in this work as a function of the distance to their nearest cluster show a strong dependence on the amount of halo substructure. Since significant halo substructure is related to ongoing or a recent merger, we could infer that the influence of the close neighbourhood of a halo in the vicinity of massive clusters is not less important than the influence of the cluster itself.

There are at least two mechanisms involved in the evolution of the shape, alignment and velocity dispersion of haloes, namely the formation time (e.g. Gottlöber et al. 2001; Sheth & Tormen 2004) and the influence of the immediate environment. In this paper we were

concerned with the latter aspect of the problem. We can summarize the interpretation of our results as follows.

On the one hand, haloes forming in high-density regions collapse earlier and they would on average have had more time to evolve and thus sphericalize, more so with respect to equal mass haloes forming in low-density regions. However, in the high-density environments an opposing factor is the overabundance of haloes which induce mergers and intrahalo interactions, which then disturb the virialized nature of these older haloes. Higher mass haloes evolve hierarchically by the accretion of lower mass haloes and thus are more elongated with respect to lower mass haloes, which collapse and form earlier according to CDM models.

The rising of the velocity dispersion of haloes (having significant substructure) near massive clusters, with respect to equal mass haloes with insignificant substructure or with those found in lower density regions, could be attributed to the higher halo merging rate present in the high-density environment of massive clusters. The fact that the fraction of haloes with significant substructure is higher in high-density regions (see end of Section 3), indeed reflects the more frequent halo mergers and interactions, which introduces also a bulk-flow (infall) velocity component in the halo velocity dispersion measure.

The merging processes in high-density environments occur along the anisotropic distribution of matter, which defines the large-scale filaments orientation. This is reflected in the alignments of the angular momenta of haloes, which are strongly influenced by the merging process, with the minor axis of the halo and the alignment of the halo major axis with the orientation of the filament, defined by the direction between the halo and its nearest massive cluster.

ACKNOWLEDGMENTS

REFERENCES

Allgood B. F., Flores A., Primack J. R., Kravtsov A. V., Wechsler R. H, Faltenbacher A., Bullock J. S., 2006, MNRAS, 367, 1781
Altay G., Colberg J. M., Croft R. A. C., 2006, MNRAS, 370, 1422
Aragón-Calvo M. A., van de Weygaert R., Jones B. J. T., van der Hulst J. M., 2007, ApJ, 655, L5
Avila-Reese V., Colín P., Gottlöber S., Firmani C., Maulbetsch C., 2005, ApJ, 634, 51
Bailin J., Steinmetz M., 2005, ApJ, 627, 647
Basilakos S., Plionis M., Yepes G., Gottlöber S., Turchaninov V., 2006, MNRAS, 365, 539
Bertschinger E., 2001, ApJS, 137, 1
Bett P., Eke V., Frenk C. S., Jenkins A., Helly J., Navarro J., 2007, MNRAS, 376, 251
Boselli A., Gavazzi G., 2006, PASP, 118, 517
Bullock J. S., 2002, in Natarajan P., ed., The Shapes of Galaxies and their Dark Matter Haloes. World Scientific Press, Singapore, p. 109
Colberg J. M., Krughoff S. K., Connolly A. J., 2005, MNRAS, 359, 272
Dressler A., 1980, ApJ, 236, 351
Dressler A., Shectman S. A., 1988, AJ, 95, 985
Dubinski J., 1992, ApJ, 401, 441
Einasto M., Einasto J., Müller V., Heinämäki P., Tucker D. L., 2003, A&A, 401, 851
Einasto M., Suhhonenko I., Heinämäki P., Einasto J., Saar E., 2005, A&A, 436, 17
Evrard A. E. et al., 2007, ApJ, submitted (astro-ph/0702241)
Faltenbacher A., Gottlöber S., Kerscher M., Müller V., 2002, A&A, 395, 1
Faltenbacher A., Gottlöber S., Mathews G., 2006, preprint (astro-ph/0609615)
Goto T., 2003, PhD thesis, Univ. Tokyo
Gottlöber S., Turchaninov V., 2006, in Mamon G. A., Combes F., Deffayet C., Fort B., eds, EAS Publ. Ser. Vol. 20, Mass Profiles and Shapes of Cosmological Structures. EDP Sciences, Les U lis Cedex A, p. 25
Gottlöber S., Klypin A., Kratsov A. V., 2001, ApJ, 546, 223
Hahn O., Porciani C., Carollo C. M., Dekel A., 2007, MNRAS, 375, 489
Hopkins P. F., Bahcall N. A., Bode P., 2005, ApJ, 618, 1
Jing Y. P., Suto Y., 2002, ApJ, 574, 538
Kasun S. F., Evrard A. E., 2005, ApJ, 629, 781
Kazantzidis S., Kratsov A. V., Zentner A. R., Allgood B., Nagai D., Moore B., 2004, ApJ, 611, L73
Knebe A., Müller V., 2000, A&A, 354, 761
Lee J., 2006, ApJ, 644, L5
Lemson G., Kauffmann G., 1999, MNRAS, 302, 111
Ma C. P., Bertschinger E., 1995, ApJ, 455, 7
Macció A. V., Dutton A. A., van den Bosch F. C., Moore B., Potter D., Stadel J., 2007, MNRAS, in press (doi: 10.1111/j.1365-2966.2007.11720.x)
Martínez H. J., Muriel H., 2006, MNRAS, 370, 1003
Maulbetsch C., Avila-Reese V., Colín P., Gottlöber S., Khalatyan A., Steinmetz M., 2007, ApJ, 654, 53
Paz D. J., Lambas D. G., Padilla N., Merchán M., 2006, MNRAS, 366, 1503
Pimbblet K. A., 2005, MNRAS, 358, 256
Pinkney J., Roettiger K., Burns J. O., Bird C. M., 1996, ApJS, 104, 1
Plionis M., 2004, in Diaferio A., ed., IAU Coll. 195, Outskirts of Galaxy Clusters: Intense Life in the Suburbs. Cambridge Univ. Press, Cambridge, p. 19
Plionis M., Basilakos S., 2002, MNRAS, 329, L47
Plionis M., Ragone-Figueroa C. J., Basilakos S., 2006, in Saviane I., Ivanov V., Borissova J., eds, ESO Astrophysics Symp., Groups of Galaxies in the Nearby Universe. Springer-Verlag, Berlin
Ragone C. J., Merchán M., Muriel H., Zandivarez A., 2004, MNRAS, 350, 983
Schuecker P., Boehringer H., Reiprich T. H., Feretti L., 2001, A&A, 378, 408
Sheth R. K., Tormen G., 2004, MNRAS, 350, 1385
Springel V., 2005, MNRAS, 364, 1105
Stoica R., Mártinez V., Mateu J., Saar E., 2005, A&A, 434, 423
Tormen G., 1997, MNRAS, 290, 411
van Haarlem M., van de Weygaert R., 1993, ApJ, 418, 544
Vitvitska M., Klypin A., Kravtsov A., Wechsler R., Primack J., Bullock J., 2002, ApJ, 581, 799
West M. J., 1994, MNRAS, 268, 79

This paper has been typeset from a TEX/LATEX file prepared by the author.